Energy Absorption Mechanisms of Nanoscopic Multilayer Structures Under Ballistic Impact Loading

Response to Reviewer #1

General Remarks: The paper studies the response of nanofilms of aluminum, polyurea and their composites to microprojectile impact using molecular dynamics simulation. This is an exciting problem to study particularly in light of the experiments showing interesting and drastically different impact responses of nanofilms. The simulation model seems to have been validated by comparing shock Hugoniot obtained from multiscale shock simulation using the model of aluminum and polyurea with the experimental data. Various parameters have been studied to gauge the response. However, often the reasons for various features in plots have not been explained and the reasons provided do not seem to be grounded in MD data or based on appropriate experiments.

Authors Response: We are grateful to the reviewer for the careful review of the manuscript and for providing us with many insightful comments, which helped us to clarify several points in the initial submission while improving its scientific contribution. In the revised manuscript, we have provided detailed explanations for the features observed in the plots, which are strongly grounded in our MD simulations. For example, we included several new figures in the manuscript (Fig. 5e to 5g, 6a, 6b) as well as in the Supplementary Information (Fig. S1 to S3) in order to explain several features that have not been properly explained in the initial submission. Our comprehensive responses (Rx) to the reviewer's comments (Cx) are given below, where we have paid careful attention to explain the features in the plots using our MD simulations. All revisions to the manuscript are highlighted in yellow.

Major Comments

C1: The manuscript has barely any information about the MD model. I believe it will be a hindrance for a reader to refer to another paper to get even the basic nevertheless crucial details about the model. So, a short paragraph about the basic details of the models of aluminum and polyurea should be added.

R1: We added the following details on page 5 of the revised manuscript.

The structure of polyurea chains used for the simulations is shown in Fig. 1a; the chain consists of 4 repeating monomers (n = 4), and each monomer has 14 soft segments (m = 14) and a hard segment. The value of m is chosen to be consistent with polyurea synthesized with Versalink® P–1000 oligomeric diamine. The molecular weight of the modeled polyurea is 6094 g/mol, where each chain consists of 976 atoms (see Fig. 1b). The contour length of a chain is 55.5 nm.

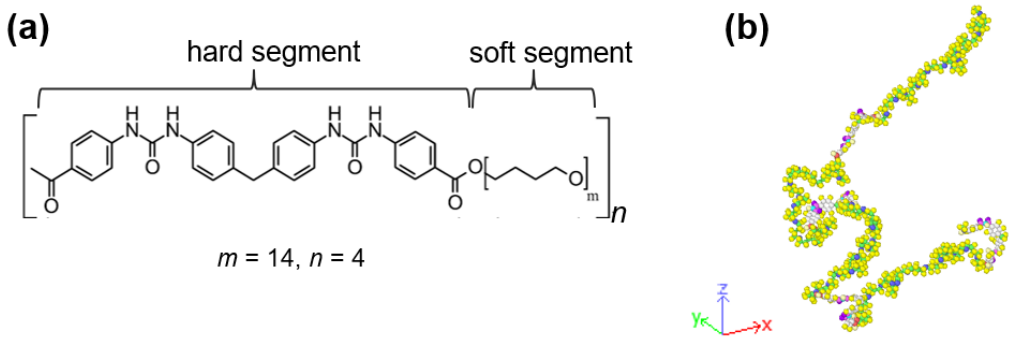

Fig. 1 Polyurea model: (**a**) Chemical structure of polyurea, where *m* is the number of repeating soft segments in a monomer, and *n* is the number of repeating monomers in a chain. (**b**) MD model of a typical polyurea chain.

The equilibration procedure of a polyurea sample has been explained in details in our previous publication [1], where the sample was initially compressed up to a density of 1.12 g/cm^3, and subsequently cured at 500 K before the final equilibration at 300 K. The final density of the sample is 1.024 g/cm^3 at 300 K under atmospheric pressure. The experimentally measured density of a comparable polyurea is approximately 1.1 g/cm^3 [2]. The slightly lower densities of our MD models may be attributed to the fact that the MD models are fully amorphous whereas some hard domains, with comparatively higher densities, prevail in the experimental samples.

Polyurea layers with three initial thicknesses (3.2 nm, 6.4 nm, and 9.6 nm) and planar dimensions of 43 × 43 nm^2 were created using the enhanced Monte Carlo package [3]. The average end-to-end polymer chain length in the smallest film is 5.2 nm, which is comparable to the thickness of the film. The largest polyurea film contains 1769 chains (i.e. 1,726,544 atoms). During the equilibration of nanofilms, the pressure components along the in-plane directions (i.e., x and y) were maintained at atmospheric pressure, and a vacuum (thickness of 5 nm) was maintained along the z-direction in order to create two free surfaces.

Thicknesses of aluminum nanofilms in multilayer structures were selected in such a way that each aluminum film has an equivalent areal density to one of the polyurea films, where the thickness of an aluminum film (t_{al}) can be expressed in terms of the thickness of a corresponding polyurea film (t_{pu}) as $t_{al} = (\rho_{pu}/\rho_{al}) \times t_{pu}$; where ρ_{pu} and ρ_{al} are the densities of polyurea and aluminum, respectively. The corresponding values of ρ_{pu} and ρ_{al} are 1.02 g/cm^3 and 2.7 g/cm^3, respectively. The corresponding three thicknesses of the aluminum films were 1.215 nm, 2.43 nm, and 3.645 nm, where the lattice constant of aluminum is 0.405 nm at 300 K according to the used EAM potential [4].

When creating composite aluminum-polyurea samples (e.g., see Fig. 2c), free surfaces of aluminum and polyurea were compressed towards their interfaces and then allowed to equilibrate

over 500,000 time steps under atmospheric pressure. More information and some LAMMPS input files to model a polymer-metal interface are available at https://github.com/nuwan-d/polymer_metal_interface.

C2: Is the dimension of the cylindrical projectile inspired by experimental projectile sizes?

R2: We included the following sentence to clarify this point (page 6).

"The diameter and height of the cylindrical projectile are 7.7 nm and 8.1 nm, respectively. It should be noted that the diameter of spherical projectiles used in microprojectile impact tests is approximately 5 μm [5–8]. In addition, macroscopic impact tests have revealed that the ballistic performance of targets depends on the geometry of the strike face of the projectile [9,10]. The effects of projectile geometry on the ballistic performance of nanoscopic targets are investigated in section 3.5."

C3: Details of polyurea are inaccurate. Experimental investigation of polyurea do not back the claim that the hard domain is crystalline. Experiments suggest very little to no crystallinity. Furthermore, the references 51, 52 are for polyurethane. Appropriate corrections should be made in section 2.2.

R3: Thank you for pointing this out. We removed the concerned discussion with the 2 references and included the following sentence in section 2.2 (page 5).

Polyurea is a segmented elastomer containing soft and hard domains where the hard-domains are embedded in a soft matrix [11,12].

C4: Why is the initial resistance independent of the thickness of the target in case of both aluminum and polyurea films? Also, is this limited to nanofilm or can it be observed in macroscale impact tests as well, if one can get sufficient time resolution? Is there any experimental result validating this observation?

R4: The initial resistance is generated by the indentation resistance of the material, where no bending of the film is involved. Yes, this phenomenon can be observed in macroscale impact tests if one can get sufficient time resolution. In fact, Nguyen et al. [13] have developed an analytical model to predict the ballistic limit velocity, V_{50}, of polymer samples where they hypothesized that a part of the kinetic energy of the projectile is spent during the initial indentation stage and another

part of the energy is spent during the bulging stage of the target. Their model has been experimentally validated and we recently used it to compute V_{50} of multilayer aluminum-polyurea layers [14]. We included the following discussion in the manuscript (page 10).

The initial contact resistance (F_c) of an isolated film is generated by the indentation resistance of the material with no film bending involved, and therefore F_c is independent of the film thickness.

C5: The appearance of accelerating force which also seems to be independent of the aluminum film thickness is puzzling. The attempt at explaining it in the first paragraph of page 11 is very confusing. That the acceleration starts at different times for different thicknesses seems to suggest that the explanation based on interaction between the elastic tensile wave and expanding cone may not be correct since all the films have the same diameter. Furthermore, it may be possible to check the stress wave propagation in the MD data, which can be used to check the accuracy of this hypothesis.

R5: Thank you for pointing this out and we agree with the reviewer. In the first paragraph of page 11, we attempted to demonstrate the same thing that the reviewer has mentioned (i.e. interaction between the elastic tensile wave and expanding cone does not cause the observed acceleration). We removed that discussion in the revised manuscript and included the following discussion on page 12.

In the case of aluminum targets, the velocity of the projectile slightly increases after the initial deceleration (see Fig. 4b). This sudden increase in the velocity can be attributed to the interaction between the advancing projectile and the tensile release wave generated by the reflection of the shock compressive wave at the back free surface of aluminum targets. Using the multiscale shock technique, we obtained the relationship between the shock speed (U_s) and the particle velocity (U_p) of aluminum, which can be given as $U_s = 5.68 + 1.38U_p$ (km/s); where the bulk sound speed is 5.68 km/s and the slope of the Hugoniot is 1.38. Based on this U_s - U_p relation, the initial impact speed of 1.5 km/s (i.e. the initial U_p of aluminum) generates a compressive shock wave propagating at a speed of 7.75 km/s, which reflects as a tensile release wave traveling approximately at the bulk sound speed. The thickness of the Al9 film is 3.645 nm, and therefore the time taken for the tensile wave to reach the projectile can be approximately computed as $(4\times3.645\times10^{-9})/[(5.68+7.75)\times10^{3}]$ = 1.08 ps, which agrees with the time taken from the initial contact to the acceleration in MD simulation that is 1.02 ps (see Fig.4b). The small discrepancy between the two periods is due to the fact that the motion of the projectile during the shock wave reverberation has not been considered in the above calculation. The projectile continues to penetrate the target during the shock wave propagation reducing the distance (and time) that the tensile release wave required to

travels in order to meet the projectile. Moreover, Fig. 4b shows that time taken from the initial contact to the acceleration is proportional to the layer thickness (i.e. 0.68 ps in Al6 and 0.32 ps in Al3), which further confirms that the observed acceleration is due to the interaction between the advancing projectile and the tensile release wave.

Shock wave reverberation occurs in polyurea films as well. The U_s - U_p relation for polyurea, obtained from MSST, can be expressed as $U_s = 2.5 + 1.7U_p$ (km/s); where the bulk sound speed is 2.5 km/s and the slope of the Hugoniot is 1.7. The projectile impact at a speed of 1.5 km/s (i.e. U_p) generates a compressive shock front in polyurea films propagating at a speed of 5.05 km/s, which reflects at the back face as a tensile release wave traveling approximately at the bulk sound speed. The thickness of the Pu6 film is 6.56 nm. Ignoring the movement of the projectile, the time taken for the tensile wave to reach the projectile can be approximated as $(4\times6.56\times10^{-9})/[(2.5+5.05)\times10^{3}]$ = 3.48 ps. However, unlike in the case of aluminum targets, the projectile travels a significant distance into the target during that period (see Fig. 4b), which needs to be taken into account. The compressive shock front reaches the back free surface of the Pu6 target after 1.3 ps from the impact. During that period, the projectile has traveled 1.92 nm into ethe sample (assuming that the target does not move during that period), and the speed of the projectile has decreased to 1.46 km/s. Therefore, the time taken for the tensile wave to reach the projectile can be computed as 1.3 + (6.56-1.92)/(2.5+1.46) = 2.47 ps. That is the approximate time when the initial contact resistance of polyurea disappears due to the arrival of the tensile release wave (marked by an arrow on the velocity profile of Pu6 in Fig. 4b). Similarly, the corresponding time for the Pu3 film is 0.65 + (3.28-0.97)/(2.5+1.486) = 1.23 ps, which also agrees with the observation made in the corresponding time-velocity profile (see Fig. 4b). The corresponding time for the Pu9 film is 1.95 + (9.84-2.86)/(2.5+1.44) = 3.72 ps.

C6: (page 9, line 46) The paragraph starting at this line is not clear. Furthermore, the line that two-stage perforation process is prominent when the arial density ratio is less than 0.08, but it does not hold for Al6 as the ratio is 0.04 seems inaccurate. Also, how would the failure mechanisms such as fiber failure and delamination in a layered material with fiber reinforcement inform the failure mechanisms in aluminum?

R6: Thank you for pointing out the typo in the sentence concerning the areal density. It should be corrected as "the two-stage perforation process is prominent when the aerial density ratio is **greater** *(not less)* than 0.08". As the reviewer pointed out, aluminum has a different failure mechanism, but it also contains a two-stage perforation process where the initial dynamic

indentation follows by excessive bending and tensile failure. We replaced that paragraph with the following sentence (page 11), which is more concise.

The observed high F_c of aluminum can be attributed to the dynamic indentation, which is associated with the dislocation movement in the target [1].

C7: Temperature rise shown in figure 4 seems to be a two-stage process for polyurea as well as aluminum. Are there specific reasons for this? Furthermore, why the maximum of the maximum pressure occurs for PU6?

R7: Thank you for bringing this up. We found that the pressure of the Pu6 film is correct, but the pressure of the Pu3 has not been properly calculated. We corrected that and did additional simulations to further explore the temperature and pressure distribution in polymer layers. We included the following discussion on page 16.

"Figures 5a and 5c show a two-stage temperature rise in all polyurea films as well as Al6 and Al9 films. In polyurea films, the plateau of the initial temperature rise occurs when the pressure of the sample is at its maximum, and the temperature continues to rise at a much slower rate until the pressure of the film completely disappears, which suggests that the adiabatic shock heating in polyurea continues until the shock pressure completely dissipates. The interchain friction can have a significant contribution to the observed post-adiabatic shock heating. The computed glass transition temperature of polyurea is 311 K (see Fig. S1 in Supplementary Information). A similar feature in the temperature rise is observed in Al6 and Al9 films, which can be related to the melting of the films. According to the EAM potential used in the current MD simulations [4], the melting temperature of aluminum is 939 K, and it increases with the pressure [15]. The plateau of the initial temperature rises of the two aluminum films occurs when the temperature is ~1200 K and the pressure is ~12 GPa, which suggests that two-stage temperature rise can be attributed to melting. However, the Al3 film shows different behavior. It should be noted that the thickness of the Al3 film is only 3 aluminum unit cells (i.e. 1.215 nm), where the surface effects are remarkably high [16].

In order to obtain further insights into the spatial variations of thermodynamic states within the Pu9 target, we investigated the evolution of temperature and pressure at three regions of the Pu9 target (see inset of Fig. 6a), where the thickness of each region is equal to that of the Pu3 target

(i.e. 3.28 nm). The maximum pressure and the rate at the top region of the Pu9 target are equal to that of Pu3 (see Fig. 6a); the pressure in the top layer of the Pu9 target is sustained for longer because of the confinement provided by the material underneath. It can be noticed that the Pu9 target starts to dissipate its pressure well even before the bottom region of the film experience any pressure; when the bottom part reaches its peak pressure, the top part has released about 50% of its peak pressure. That pressure dissipation mainly comes from lateral migration of polymer chains (see Supplementary Movie M1). It can also be noted that the pressure dissipation rate of the top part decreases as the bottom part reaches its maximum pressure (~5.5 ps). At that time, the entire film underneath the projectile is under a significant shock compression, which makes the pressure dissipation through polymer chain migration difficult, and therefore the pressure is sustained comparatively longer. The initial rapid pressure release of the top and bottom layers is due to the fact that the polymer chains at the surfaces are highly mobile compared to the interior chains. The lower pressure reduction rate of the middle layer confirms this hypothesis. The top region of the Pu9 target is under significant compression when the tensile release wave reaches the projectile, which could be attributed to the fact that polymer chains are trapped underneath the projectile, and they can only be released once they have drawn out of the melt. The temperature rate at the top region of the Pu9 target is equal to that of Pu3, but the adiabatic heating of the Pu9 targets through relative sliding of polymer chains continues longer (see Fig. 6b).

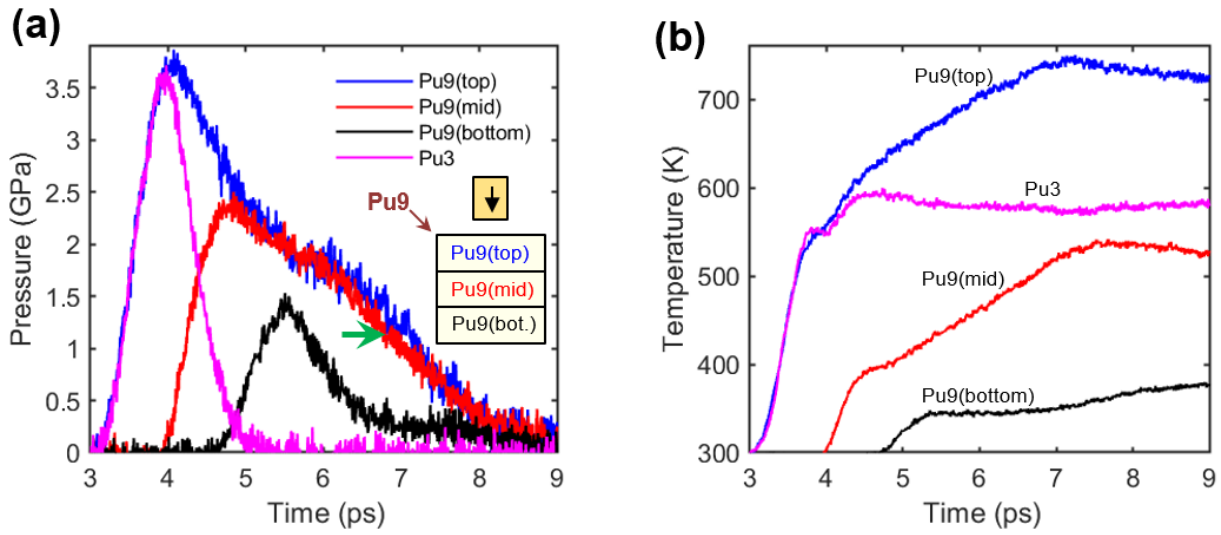

Fig. 6 Temporal variations of (**a**) temperature and (**b**) pressure underneath the projectile in Pu9 and Pu3 targets, where the temperature and pressure of the Pu9 target were obtained in three separate regions, with the thickness of each being equal to that of the Pu3 target (see inset of Fig. a). The green arrow indicates the computed time when the tensile release wave reaches the projectile."

In addition, we included the following discussion on page 16 to explain some features in Fig. 5.

"The arrival time of tensile release waves, computed from the shock wave speeds in section 3.2.1, is indicated by the green arrows in Fig. 5. When the tensile release wave in the aluminum targets reaches the penetrating projectile, the pressure underneath the projectile dissipates, except for the case of the Al3 target that can be attributed to the extremely thin nature of the target and the cohesion between the target and projectile. However, the compression of the polyurea films does not dissipate at the arrival of the tensile release wave. That may be attributed to the fact that the sharp edge of the blunt-nosed projectile can trap several polymer chains and put them under a high compressive state, which cannot be released by the tensile release wave alone. The pressure in the Pu3 film is comparatively higher when the release wave arrives because the number of trapped polymer chains compared to the other polymer chains is high in Pu3. Figures 5e to 5g show cross-sectional view, going through the center of the three polyurea samples, at the time when the pressure of the targets completely disappears."

Furthermore, we included the following discussion on page 20 to explain some features in Table 3.

"However, energy dissipation through instantaneous adiabatic heating and internal energy change in the polyurea films is significantly smaller than the corresponding energies dissipated by the aluminum films (see Table 3). The polymer films dissipate a much larger portion of energy through extensive melt drawing (see Fig. 4d). When the thickness of the polymer films decreases, the films experience higher temperature facilitating melt drawing, which leads to a reduction in the energy dissipation through melt drawing. Uniaxial tensile tests conducted at temperatures from 200 K to 500 K showed a remarkable reduction in the yield stress of polyurea with temperature (see Fig. S2 and Table S1 in Supplementary Information)."

C8: Are Cp used for polyurea and aluminum estimated at the maximum pressures observed in the simulation? If not, it should be mentioned in the text as a limitation.

R8: We included the following sentence on page 16.

The values of C_p were obtained from the existing experimental studies, which are ~2500 J/Kg-K and 910 J/Kg-K for polyurea and aluminum, respectively [12,17].

C9: The area experiencing severe deformation seem to be very different for aluminum and polyurea, based on the images in figure 3. But line 42 on page 13 assumes them to be equal. Can't MD data be used to obtain an estimate for the two materials and thicknesses based on some measure of strain in MD?

R9: To clarify this point, we included the following discussion on page 16 of the manuscript.

The areas experiencing severe deformation in aluminum and polyurea films are significantly different as the projectile completely penetrates the corresponding targets (see Fig. 4c and 4d when t = 25 ps). However, the temperature and pressure rise within ~1 ps from the initial contact (see Fig. 5), where our MD simulations reveal that the area experiencing severe deformation in both films is approximately equal to twice the strike face area of the projectile.

C10: In figure 6a (also in fig 8a), Fi for Al3_Pu3 seems to have been calculated inaccurately. The initial slope seems close to Al6. Also, the initial slope was shown to be independent of film thickness earlier in the paper.

R10: As the reviewer pointed out in comment C13, this confusion is because F_i and F_s have not been properly defined. Now we have clearly defined the three resisting forces, which are the contact force (F_c), initial resisting force (F_i), and secondary resisting force (F_s).

(page 10): The initial contact resistance (F_c) of an isolated film is generated by the indentation resistance of the material with no film bending involved, and therefore F_c is independent of the film thickness.

(page 23): In order to compare the penetration resistance in multilayer targets made of different numbers and arrangements of Al3 and Pu3 films, we define the initial resisting force (F_i) and secondary resisting force (F_s), which are motivated by the two prominent gradients in the time-velocity curves of penetrating projectiles. The value of F_i is somewhat similar to F_c in isolated films (defined in section 3.2), but F_i has a minor contribution from the bending stiffness provided by the underneath films. The definition of F_s is similar to that of an isolated film (see section 3.2.1).

C11: In figure 6b, Al in Al3_Pu3 has a negative pressure in the beginning, like observed in pure aluminum films as well. That disappears in the case of Pu3_Al3. Why does that happen?

R11: We included the following sentences to explain this observation.

(page 14): "It can be observed in Fig. 5d that aluminum films experience a negative pressure just before the initial contact. That is due to the fact that the non-bonded interaction between the projectile and the aluminum target pulls the target towards the projectile generating tensile stress (i.e. negative pressure) in the sample. The non-bonded interaction between the polymer and the projectile is not strong enough to generate a significant pulling and therefore polyurea films do not experience a negative pressure. The maximum pressure experience by the polymer films significantly increases as the thickness decreases (see Fig. 5c), which can be attributed to the fact that the propagating shock wave in narrow polymer films rapidly increases the shock pressure, allowing a limited time for the polymer chains to migrate laterally and release some pressure. The initial temperature (dT/dt) and pressure (dP/dt) rates of polyurea are almost independent of the target thickness. However, (dT/dt) and (dP/dt) of Al3 is slightly higher than those of Al6 and Al9, which could also be attributed to the fact that the Al3 target is only 3 aluminum unit cells thick. For the Pu9 film, (dT/dt) and (dP/dt) are177×10^{12} K/s and 2×10^{12} GPa/s, respectively. For the Al9 film, (dT/dt) and (dP/dt) are 3040×10^{12} K/s and 42.8×10^{12} GPa/s, respectively."

(page 25): "The aluminum film in Al3_Pu3 experiences a negative pressure just before the initial contact, which is due to the adhesion between aluminum and the projectile as explained in section 3.2.1. The negative pressure disappears in the case of Pu3_Al3, where the projectile first comes into contact with the polyurea layer, and the aluminum layer experiences shock pressure through the polymer even before the projectile reaches aluminum."

C12: Based on figure 7, failure in Pu in Al3_Pu3 appears to be tensile failure unlike in Pu in Pu3_Al3 where it appears to be shear plugging. Could that be one of the reasons for relatively poor performance of Al3_Pu3?

R12: Yes, we agree with the reviewer; we included the following discussion on page 23 of the revised manuscript.

"Moreover, Different failure mechanisms can be observed in the Pu3 film of the multilayers Al3_Pu3 and Pu3_Al3, which also contributes to the difference in their ballistic performance. The Pu3 film of Pu3_Al3 demonstrates shear plugging (see Fig. 8c), whereas the Pu3 film of Al3_Pu3

demonstrates more tensile-like failure (see Fig. 8d). Particularly, in the case of Al3_Pu3, the initial impact between the projectile and Al3 film generates a propagating shockwave, which reaches the Pu3 film before the advancing projectile because the shock compressive wave travels at a speed of 7.75 km/s (see section 3.2.1). That shock compressive wave reflects at the back free surface of Pu3 as tensile release wave generating tensile stress in the Pu3 film making it weaker."

In addition, we included the following discussion on page 25 to explain some features in Fig. 8.

"The underneath Pu3 layer of the Al3_Pu3 target starts experiencing the shock pressures as soon as the Al3 layer at the strike face reaches its maximum pressure (indicated by a dashed-blue vertical line in Fig. 8b). However, the underneath Al3 layer of the Pu3_Al3 target start experiencing the shock pressures well before the Pu3 reaches its maximum pressure, and in fact pressure of the Al3 layer drops even before the Pu3 reaches its maximum. This observation can be attributed to comparatively higher impedance (Z) of aluminum; $Z = \rho_0 U_s$, where ρ_0 is the initial density of the material and U_s is the shock wave speed. Pressure transmission and reflection at an interface depends on the impedance of the two materials; when a shock wave traveling through a material (e.g., polyurea) encounters an interface with another material with a higher impedance (e.g., aluminum), the shock pressure of the material with the lower impedance further increases [18]. During the time between the two arrows marked in Fig. 8b, the shock wave has traveled through the Pu3, and the computed U_s is 4.69 km/s, which is slightly lower than the value given by the Hugoniot U_s - U_s relations for the bulk material (i.e. 5.05 km/s). This reduced U_s can be due to the presence of a free surface and an interface in the material sample. Similarly, the computed U_s for aluminum is 7.15 km/s, which is also slightly smaller than the value given by the Hugoniot U_s - U_s relation (i.e. 7.75 km/s)."

Similarly, we included the following discussion on page 28 to explain some features in Fig. 9.

"Using the arrival times of the shock compression waves at the interior layers of the Al3_Pu3_2 target (marked by arrows in Fig. 9b), a direct estimate of the shock wave speeds in the Pu(mid) and Al(mid) layers can be obtained, which are 6.37 km/s and 4.76 km/s, respectively. It shows that Pu3(mid) layer, which is confined between 2 aluminum layers, experiences higher shock velocity than when it is being impacted directly, and the shock pressure is sustained over a significantly long time. As shown in the inset of Fig. 9c (t = 12.5 ps) some polymer material is trapped between the projectile and the Al(mid) layer, which disturbs the dissipation of shock pressure."

C13: It is unclear what criteria has been used to define Fi and Fs. In all cases with Al at the top, Fi appears to be close to Fi for pure Al from the velocity vs time plots. Yet, the results reported for composites in figure 12a are very different from pure Al films.

R13: Thank you for pointing out this confusion. We have now defined Fi and Fs, which are given in our response to C10.

C14: The discussion on comparison of the simulation results with experiments (page 25, second paragraph) misses two important points that must be highlighted in the discussion: large differences in strain rates and the fact that there is no polyurea chain scission indicating chain lengths are not long enough in simulation to cause entanglement. Sufficient chain entanglement has been experimentally observed in nanofilm impact to lead to an improvement in dissipation. It seems reasonable to think that in that case polyurea on the back face will not perform as badly as it does right now when chains can easily slide and disentangle. Furthermore, this is also one of the reasons that made me suggest to specify basic details of the model such as chain length/molecular weight in this paper.

R14: We agree with the reviewer and included the following paragraphs just below the concerned paragraph (page 34).

"Moreover, the molecular weight of polyurea used in the current study (i.e. 6094 g/mol) is significantly smaller than the molecular weight of the polymers used in many experimental studies. For example, the molecular weight of ultrathin polymer films (thickness ~100 nm) used for recent microprojectile impact tests is typically ~30,000 g/mol, but it can even be over 250,000 g/mol for some cases [5,7,19,20]. The smaller chain size used in the current study to limit the computational cost could results in a relatively lower entanglement leading to poor performance of polyurea-backed aluminum films because the lower entanglement of polymer chains results in a lower tensile load carrying capacity. Microprojectile impact tests have revealed that the failure mechanism and the size of the plastic deformation zone of ultra-thin polycarbonate and polystyrene films depend on the entanglement density [7,20].

The mechanical behavior of materials significantly depends on the strain rate. For example, experiments conducted on polyurea at various compressive strain rates, ranging from 10^{-3} s^{-1} to 1.5×10^{4} s^{-1}, have revealed that the energy absorption capacity of the polymer significantly increases with the strain rate due to the dynamics of polymer chains [21–23]. In fact, we conducted

uniaxial tensile and compressive tests of polyurea samples with strain rates of 10^8 s^{-1}, 10^9 s^{-1}, and 10^3 s^{-1}, which showed that the corresponding yield stress significantly increases as the strain rate increases (see Fig. S3 and Table S2 in the Supplementary Information). The strain rate in our MD simulations can be a few orders of magnitude higher than the corresponding experimental strain rates of macroscopic plates, which can have a significant influence on the observed superior performance of the nanoscopic multilayers. It should also be noted that the strain rates in microprojectile impact tests can be as high as 10^{10} s^{-1} [8,24], which are in the order of strain rates reported in this paper (see Table S3 Supplementary Information)."

C15: In line 38, page 26, the pattern in the plot in figure 13 has been reasoned to indicate that at macroscale metal plates with polyurea at the back could become better at resisting impact. It has to be recognized that there is large scale different between the current simulation and macroscale experiments and extrapolation of these results to macroscale is not fraught with challenges. So, adding this caveat to the current reasoning in line 38 would be appropriate.

R15: As the reviewer suggested, we included the following sentences just after the concerned sentence (page 35).

"However, it should be noted that there is a large length scale difference between the current MD simulations and macroscale experiments, and therefore extrapolation of current MD results to macroscale faces several challenges. For example, sliding and fragmentation of hard domains in domain segregated macroscopic polyurea samples can significantly contribute to the energy dissipation under impact loading. Moreover, defects and complex grain boundary structures of macroscopic metal targets can also play a significant role in absorbing impact energy."

C16: Based on figure 6a, the point corresponding to Al6 in the specific penetration energy plot in figure 13 seems to be incorrect. Figure 6a suggests that specific penetration energy for Al6 should be highest among Al6, Al3_Pu3 and Pu3_Al3. Furthermore, the supremacy of pure Al nanofilms in comparison to composites suggests that for the same mass of the film, they perform better than composites. So, does it not effectively suggest that the effort to design such composites for impact resistance is not a fruitful exercise?

R16: Please note that, as mentioned in the caption of Fig. 13 (Fig. 14 in the revised manuscript), we measured the residual velocity when the time is 60 ps. The complete time-velocity plot is only shown in Fig. 4a, and the other figures including Fig. 6a (Fig. 7a in the revised manuscript) show only a part of the velocity profile (up to ~30 ps), where the profile changes significantly. The

corresponding full time-velocity plot is shown below. Moreover, please note that the mass of the target material attached to the projectile (m_{plug}) is also important in computing the specific penetration energy (please see Eq. (3)) and Fig. 8c shows that m_{plug} of Pu3_Al3 is significantly high. We confirm that Fig. 13 is correct.

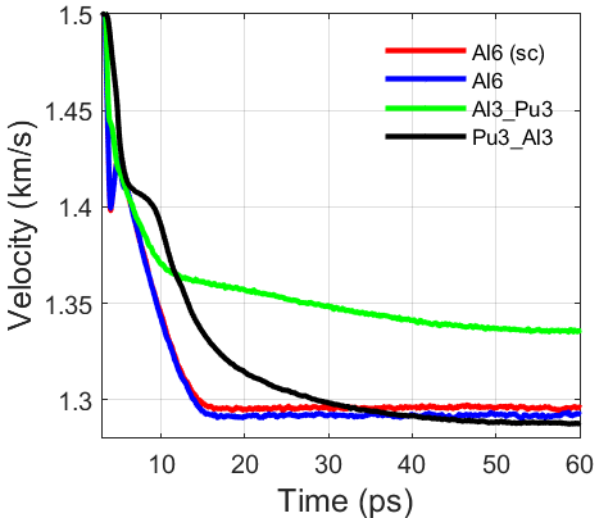

In response to the reviewer's comment on the supremacy of pure Al nanofilms, we included the following discussion on page 36.

"The traditional body armors are typically designed by using ultra-strong yet high stiff materials to stop advancing projectiles, and therefore those armors are stiff. The major limitation of polymer-based soft body armors is that the polymeric materials required to undergo large deformations to absorb impact energy, and such deformations can induce nonpenetrating injuries [25,26]. The observed high impact resistance of the nanoscale multilayers suggests that it may be possible to design more flexible armors from a barrier material made of nanoscopic polymer/metal films."

Minor Comments

CM1: The paper neither proposes multiscale shock technique nor shows the comparison between the simulated and experimental shock Hugoniot for aluminum or polyurea for the first time. So, it would be appropriate to modify lines 29, 30 in the introduction to reflect that the comparison has been made to validate further simulation results.

RM1: We agree with the reviewer and removed the sentence from the abstract: "Using the multiscale shock technique, we demonstrated that MD simulations can be successfully used to reproduce the experimental shock Hugoniot of polyurea."

CM2: In line 58, page 1, some references should be added.

RM2: We included these four references [27–30].

CM3: (line 41, page 7), Reed et al. proposed appropriate constraints to MD based on Euler equations.

RM3: The corrected sentence now reads as "By applying appropriate constraints to MD simulations based on Euler equations, Reed et al. [61] proposed …".

CM4: It is unclear what the second paragraph on page 11 is aimed to convey. It seems out of place to me. Perhaps authors can reframe it.

RM4: That paragraph is aimed to convey the fact the strain rates in microprojectile impact tests are approaching the strain rates reported in the manuscript. We removed that paragraph from page 11 and incorporated it into our response to the reviewer's comment C14.

CM5: In page 14, line 24, does 'polymer chains attached to the projectile' means the polymer chains in direct contact with the projectile?

RM5: Those are the polymer chains that are taken out from the target by the projectile. We clarify this point in the manuscript.

References:

[1] M.A.N. Dewapriya, R.E. Miller, Molecular Dynamics Study of the Mechanical Behavior of Ultrathin Polymer Metal Multilayers Under Extreme Dynamic Conditions, Comput. Mater. Sci. 184 (2020) 109951. https://doi.org/10.1016/j.commatsci.2020.109951.

[2] W. Mock, S. Bartyczak, G. Lee, J. Fedderly, K. Jordan, M. Elert, M.D. Furnish, W.W. Anderson, W.G. Proud, W.T. Butler, DYNAMIC PROPERTIES OF POLYUREA 1000, in: Nashville (Tennessee), 2009: pp. 1241–1244. https://doi.org/10.1063/1.3295029.

[3] P.J. In 't Veld, Enhanced Monte Carlo, 2019. http://montecarlo.sourceforge.net/emc.

[4] F. Ercolessi, J.B. Adams, Interatomic Potentials from First-Principles Calculations: The Force-Matching Method, Europhys. Lett. EPL. 26 (1994) 583–588. https://doi.org/10.1209/0295-5075/26/8/005.

[5] J. Cai, R. Thevamaran, Superior Energy Dissipation by Ultrathin Semicrystalline Polymer Films Under Supersonic Microprojectile Impacts, Nano Lett. 20 (2020) 5632–5638. https://doi.org/10.1021/acs.nanolett.0c00066.

[6] J.-H. Lee, P.E. Loya, J. Lou, E.L. Thomas, Dynamic mechanical behavior of multilayer graphene via supersonic projectile penetration, Science. 346 (2014) 1092–1096. https://doi.org/10.1126/science.1258544.

[7] E.P. Chan, W. Xie, S.V. Orski, J.-H. Lee, C.L. Soles, Entanglement Density-Dependent Energy Absorption of Polycarbonate Films via Supersonic Fracture, ACS Macro Lett. 8 (2019) 806–811. https://doi.org/10.1021/acsmacrolett.9b00264.
[8] J. Hyon, M. Gonzales, J.K. Streit, O. Fried, O. Lawal, Y. Jiao, L.F. Drummy, E.L. Thomas, R.A. Vaia, Projectile Impact Shock-Induced Deformation of One-Component Polymer Nanocomposite Thin Films, ACS Nano. 15 (2021) 2439–2446. https://doi.org/10.1021/acsnano.0c06146.
[9] X. Huang, W. Zhang, Y. Deng, X. Jiang, Experimental investigation on the ballistic resistance of polymer-aluminum laminated plates, Int. J. Impact Eng. 113 (2018) 212–221. https://doi.org/10.1016/j.ijimpeng.2017.12.002.
[10] I. Mohagheghian, G.J. McShane, W.J. Stronge, Impact perforation of polymer–metal laminates: Projectile nose shape sensitivity, Int. J. Solids Struct. 88–89 (2016) 337–353. https://doi.org/10.1016/j.ijsolstr.2016.01.010.
[11] A.M. Castagna, A. Pangon, T. Choi, G.P. Dillon, J. Runt, The Role of Soft Segment Molecular Weight on Microphase Separation and Dynamics of Bulk Polymerized Polyureas, Macromolecules. 45 (2012) 8438–8444. https://doi.org/10.1021/ma3016568.
[12] D. Fragiadakis, R. Gamache, R.B. Bogoslovov, C.M. Roland, Segmental dynamics of polyurea: Effect of stoichiometry, Polymer. 51 (2010) 178–184. https://doi.org/10.1016/j.polymer.2009.11.028.
[13] L.H. Nguyen, S. Ryan, S.J. Cimpoeru, A.P. Mouritz, A.C. Orifici, The effect of target thickness on the ballistic performance of ultra high molecular weight polyethylene composite, Int. J. Impact Eng. 75 (2015) 174–183. https://doi.org/10.1016/j.ijimpeng.2014.07.008.
[14] M.A.N. Dewapriya, R.E. Miller, Superior Dynamic Penetration Resistance of Nanoscale Multilayer Polymer/Metal Films, J. Appl. Mech. 87 (2020) 121009. https://doi.org/10.1115/1.4048319.
[15] J. Ma, W. Li, G. Yang, S. Zheng, Y. He, X. Zhang, X. Zhang, X. Zhang, Modeling the pressure-dependent melting temperature of metals, Phys. Earth Planet. Inter. 309 (2020) 106602. https://doi.org/10.1016/j.pepi.2020.106602.
[16] R.E. Miller, V.B. Shenoy, Size-dependent elastic properties of nanosized structural elements, Nanotechnology. 11 (2000) 139.
[17] J.G. Kaufman, Fire resistance of aluminum and aluminum alloys: & measureing the effects of fire exposure on the properties of aluminum alloys, ASM International, Materials Park, OH, 2016.
[18] R.M. Elder, T.C. O'Connor, T.L. Chantawansri, Y.R. Sliozberg, T.W. Sirk, I.-C. Yeh, M.O. Robbins, J.W. Andzelm, Shock-wave propagation and reflection in semicrystalline polyethylene: A molecular-level investigation, Phys. Rev. Mater. 1 (2017) 043606. https://doi.org/10.1103/PhysRevMaterials.1.043606.
[19] J. Hyon, O. Lawal, O. Fried, R. Thevamaran, S. Yazdi, M. Zhou, D. Veysset, S.E. Kooi, Y. Jiao, M.-S. Hsiao, J. Streit, R.A. Vaia, E.L. Thomas, Extreme Energy Absorption in Glassy Polymer Thin Films by Supersonic Micro-projectile Impact, Mater. Today. 21 (2018) 817–824. https://doi.org/10.1016/j.mattod.2018.07.014.
[20] W. Xie, J.-H. Lee, Dynamics of Entangled Networks in Ultrafast Perforation of Polystyrene Nanomembranes, Macromolecules. 53 (2020) 1701–1705. https://doi.org/10.1021/acs.macromol.9b02265.
[21] X. Zhang, J. Wang, W. Guo, R. Zou, A bilinear constitutive response for polyureas as a function of temperature, strain rate and pressure, J. Appl. Polym. Sci. 134 (2017) 45256. https://doi.org/10.1002/app.45256.
[22] H. Guo, W. Guo, A.V. Amirkhizi, R. Zou, K. Yuan, Experimental investigation and modeling of mechanical behaviors of polyurea over wide ranges of strain rates and

temperatures, Polym. Test. 53 (2016) 234–244. https://doi.org/10.1016/j.polymertesting.2016.06.004.
[23] H. Wang, X. Deng, H. Wu, A. Pi, J. Li, F. Huang, Investigating the dynamic mechanical behaviors of polyurea through experimentation and modeling, Def. Technol. 15 (2019) 875–884. https://doi.org/10.1016/j.dt.2019.04.016.
[24] X. Wang, M. Hassani, Ultra-High Strain Rate Constitutive Modeling of Pure Titanium Using Particle Impact Test, J. Appl. Mech. 87 (2020) 091007. https://doi.org/10.1115/1.4047290.
[25] L. Cannon, Behind Armour Blunt Trauma - an emerging problem, J. R. Army Med. Corps. 147 (2001) 87–96. https://doi.org/10.1136/jramc-147-01-09.
[26] J. Cai, R. Thevamaran, Superior Energy Dissipation by Ultrathin Semicrystalline Polymer Films Under Supersonic Microprojectile Impacts, Nano Lett. (2020) acs.nanolett.0c00066. https://doi.org/10.1021/acs.nanolett.0c00066.
[27] W. Xia, J. Song, Z. Meng, C. Shao, S. Keten, Designing multi-layer graphene-based assemblies for enhanced toughness in nacre-inspired nanocomposites, Mol Syst Eng. 1 (2016) 40–47. https://doi.org/10.1039/C6ME00022C.
[28] A.R. Alian, M.A.N. Dewapriya, S.A. Meguid, Molecular dynamics study of the reinforcement effect of graphene in multilayered polymer nanocomposites, Mater. Des. 124 (2017) 47–57. https://doi.org/10.1016/j.matdes.2017.03.052.
[29] Y. Cui, N. Li, A. Misra, An overview of interface-dominated deformation mechanisms in metallic nanocomposites elucidated using in situ straining in a TEM, J. Mater. Res. 34 (2019) 1469–1478. https://doi.org/10.1557/jmr.2019.66.
[30] S. Clifton, B.H.S. Thimmappa, R. Selvam, B. Shivamurthy, Polymer nanocomposites for high-velocity impact applications-A review, Compos. Commun. 17 (2020) 72–86. https://doi.org/10.1016/j.coco.2019.11.013.